Feasibility of Algal Biochar, a Byproduct of Biofuels Production, as a Supplemental Cementitious Material

Lan Li[a], Zihao Li[a], Chao Zeng[a], Jing Wu[a], Yuntian Teng[b], Mark Rhodes[a], Jarrod Crum[a], Andrew Schmidt[a], Peter J Valdez[a], Carlos A Fernandez[a*]

[a]Pacific Northwest National Laboratory, 902 Battelle Blvd., Richland, WA, 99354, USA

[b]Stevens Institute of Technology, 1 Castle Point Terrace, Hoboken, NJ, 07030, USA

∗ Corresponding author. E-mail address: carlos.fernandez@pnnl.gov

▪ Abstract

Algal biochar, as the solid residue of biofuel production from algal biomass, is reported to explore disposition options, aiming to lessen the liability or obstacles to biofuel production processes. However, landfill and open combustion lead to adverse environmental impacts. One way to add value to such wastes is by using them as admixtures in cementitious construction materials. This study aims to investigate the feasibility of algae-derived biochar as supplementary cementitious materials at different water content and mixture ratio. Algal biochar-cement composites were prepared with different algal biochar content, different as well as different water-to-cement (w/c) ratios and the surface area, morphology, elemental and mineralogical composition characterized. To compensate for the high-water absorption of algal biochar a small concentration of a superplasticizer was used since higher w/c ratios negatively impact strength. Mechanical performance of algal biochar-cement composites is compared with control composites using commercial silica fume as a typical commercial SCM. The findings suggest that algal biochar is a promising candidate to replace commercial SCM, like silica fume since algal biochar-cement composites can reach comparable compressive strength and Young's modulus to commercial pozzolan-cement materials with the same w/c ratio though at later curing times, 33 days. Although the tensile strength of algal biochar-cement composites is statistically similar at 7 days, it is significantly lower at later curing times and further investigation is required to improve this property. Algal biochar-based cement binders showed comparable embodied carbon as silica fume-based cement binders based on a cradle-to-gate lifecycle analysis. However, the ability of algal biochar to absorb large volumes of CO_2 over short periods of time, as measured in this study, makes this novel SCM an excellent alternative to reduce embodied carbon of concrete structures cradle-to-grave at 1/10 of the cost. Valorization of algae-derived solid waste provides great potential to reduce embodied carbon and brings credit to biofuel production and concrete-based construction.

▪ Introduction

Hydrothermal liquefaction (HTL) is suggested to be a flexible, robust and economically viable technology to produce biofuels from wet biomass, such as algal biomass, organic waste and wastewater sludges [1]. In addition to the biofuel, HTL process also produces non-condensable gas, solid and aqueous byproducts. Aqueous and gas byproducts can be fully valorized by pretreatment and recycling. However, the processing of solid residue emerges as a pressing problem due to the large yield and complex compositions in pilot-scale HTL process. A mature commercial HTL plant would produce a solid output stream exceeding 20 wt%, as predicted by modeling [2]. Composition analysis of select solid wastes presents a breadth of inorganic metals including heavy metals which would arise toxin in landfill disposal[3]. According to the State of Technology assessment by U.S. Department of Energy, landfill disposal is the default method for handling

solid wastes generated by a projected large-scale commercialized HTL process [2]. Other valorization options have also been explored, such as direct utilization as fertilizer [4] and soil amendment [5] or utilization of specific constituents by struvite recovery [6]. However, the large variability of nutrient elements (i.e., P, K, and N) from different feedstocks negates the value of HTL solid wastes and potentially increase the liability to commercialization. In addition, the heavy elements (i.e., Zn, Cu, Ni, Mo and Cr) and hazardous elements (i.e., F, K, P and U) in solid byproducts arise serious environmental concerns. Even though partial valorization produces value-added advantage, for commercial implementation, there must be a final disposition plan in place for the remaining residual material.

An alternative means to fully valorize solid wastes from HTL process can be achieved by using them as mineral admixture in cementitious composites. The demonstrated solid residue collection by solvent extraction step for continuous flow HTL is comprised mainly of ash and char[3]. In this study, we adopted the terminology used in literature reference[3, 7]. The organic residue is termed 'char', the inorganic solid is termed 'ash', and the mixture of char and ash is termed 'biochar', irrespective of the significant variation in organic carbon content present in different HTL solid wastes[3]. Ash accounts for above 55 wt %, and preferably near 80 wt % of the solid residue from various feedstock sources [3]. The major advantage of using biochar as a mineral admixture in cementitious composites stems from its superior compatibility with chemical minerals. Depending on feedstock and thermochemical conversion, biomass-derived ash contains high content of alkaline-earth element (i.e., Ca and Mg)[8]. The content of MgO and CaO could be as high as 16.12% and 83.46% in certain biomass-derived ash [9]. These carbon reactive minerals pose great potential to absorb atmospheric CO_2 as admixture in cementitious materials. The high fraction of silica (i.e., up to 94.48%) provides extra merits in pozzolanic reaction for cement strength enhancement[10]. In addition, the heavy metal and hazardous elements in biochar can be immobilized in the sediment products to avoid environmental issue from landfill disposal[11]. Therefore, using biochar-supplemented cementitious composites in construction can transform future buildings into carbon sinks, thereby reducing the overall environmental impact of concrete manufacturing and construction[7].

Other advantages of biochar lie in its economic feasibility and relatively high yield as supplementary cementitious materials (SCM). SCM are mainly used to partially replace cement in concrete industry and reduce CO_2 emission from kiln calcination. The most widely used SCM include silica fume, fly ash and blast furnace slag. These SCM are pozzolanic substances that react with calcium hydroxide to form aluminum- or silicon-containing hydraulic compounds, thereby enhancing the strength of cement-based composites. Their substitution cost for clinker is estimated to be \$42, \$55 and \$500 per ton, respectively [12]. Fly ash and blast furnace slag have limited supply with 40.8 and 17 million tons per year in United States; silica fume is prohibitively expensive for widespread use. What's more, the increasing environmental concern drives the declining annual supply of fly ash and blast furnace slag from coal-fired power plant. In contrast, the supply of dry biochar has potential to increase from current 80 million tons per year (assumed 20% biochar yield [13]) to 300 million tons per year in United States [14]. Currently, the biochar has no beneficial commercial re-use and is disposed of at special landfills at a cost of \$55 per ton, which is estimated based on national average solid waste disposal cost [15] . The use of aluminum, calcium, silica-rich biochar could provide significant value to these solid wastes as a new supply of SCMs.

Biochar is typically sourced from algae biomass, forest and wood waste, urban organic waste, agricultural waste, and more. Agricultural waste, along with wood and forest waste, is collectively referred to as lignocellulosic biomass. Extensive research over the past several decades has focused on lignocellulosic biochar as a mineral admixture in cement. In those studies, it is common to observe that lignocellulosic biochar substitutes a small portion of cement to reduce its usage in the mixture. For instance, rice husk ash substitutes 5 wt% of cement to enhance the late-age strength and durability of concrete[16]. Biochar from

wood sawdust incorporates 2 wt% as a carbon-sequestering additive in cement mortar[7]. Hardwood-derived biochar replaces 5 wt% of cement to reduce its usage[17]. Hazelnut shell-derived biochar employs 0.8-1.0 wt% as microaggregates to improve compressive strength, bending strength and fracture energy of cement paste[18]. Biochar from rice husk, sewage sludge and wood chips exhibits a strong sorption affinity of hydrophobic organic compounds[19]. Coconut shell-derived biochar, with 0.08 wt%, acts as an additive to significantly enhance the compressive strength and fracture toughness of cement paste[20]. For a comprehensive review of the function and additions of biochar in cement and concrete materials, refer to reviews by Akinyemi et al and Legan et al[21, 22]. The physicochemical properties of biochar, along with its effectiveness as a cementitious admixture, are determined by the type of waste biomass used in its production. Although lignocellulosic biochar has been explored as a potential SCM, its availability may not be sufficient to meet the demands of the construction industry in certain regions. Consequently, it is crucial to explore a broader range of biochar types to ensure that readily available solid wastes can be used to produce greener and more cost-effective cementitious materials. Given the growing importance of algae as a biofuel source, algal biochar should also be considered as a mineral admixture.

Algae-derived biopolymers have traditionally been used as agents for controlling volume changes during hydration and viscosity modifiers in cement formulations [23, 24]. Additionally, the inclusion of unprocessed algal biomass, whether in the form of intact tissues or cells, as polymeric matrices or filler materials, has been explored. For example, two types of unprocessed algal biomass have been added to ordinary portland cement at concentrations ranging from 0.5% to 15% by weight [25]. An addition of both unprocessed and pretreated algal biomass at concentration of 0.3-3 wt% to cement are analyzed [26]. In their follow-up work [27], the algal biochar is doped with metals (zinc and calcium) to prepare nanocomposite particles. 3 wt % algal biochar-zinc and agal biochar-calcium nanocomposite particles are used to tailor the reaction kinetics and compressive strength of cement paste. These prior works have focused on understanding the effects of organics in algal biomass or biochar on cement hydration at low concentrations. Introducing low concentration of these waste materials to cement provides little value to the massive disposal of algae-derived solid waste. It is important to explore the performance of cement composites with this high fraction of algal biochar to reduce the carbon footprint of cement and the cost of commercial SCMs and pozzolans without affecting mechanical and rheological properties of the cementitious materials. Nevertheless, to the best of our knowledge, the feasibility of algal biochar as a significant (i.e., 30 wt%) replacement of cement in the mortar has not been reported yet.

To this end, the present study aims to investigate the effect of large addition (30 wt%) of biochar produced from algae by HTL process as a waste based SCM. The effect of the algal biochar on hydration kinetics, mechanical strength, and microstructure of cement composites are analyzed. In addition, the comparison with commercial silica fume has been conducted at different water-to-cement ratio and biochar-to-cement ratio in search for the optimal composition of the mortars.

▪ Materials and Methods

Materials. The algal biochar used in this study was derived from HTL of a biomass slurry consisting of a microalgae and fine sawdust. The microalgae were harvested as dilute slurry of a mixed algae bloom on Harsha Lake (in Clermont County, Ohio in September 2022). The algae bloom was not speciated. To reduce the slurry volume and to provide a solids concentration that was amenable to HTL processing, the algal biomass was thickened to a paste. Thickening involved a dissolve air flotation system and a screw press. Sawdust sourced from a local sawmill was added as a thickening agent in a concentration of 25 wt% on a dry basis. The final slurry is typical of blended feedstocks that are evaluated for HTL. Detailed characterization of the biomass slurry was performed with a summary of the results in Table 1. Prior to the

HTL processing, Na_2CO_3 was added at 10 grams to each kilogram of slurry (1 wt%) to serve as a buffering agent for the HTL reaction chemistry. The final concentration of solids in the feed slurry was 14.4 wt%. The sample was processed in the continuous flow HTL reactor at a residence time of 14 minutes and reactor temperature of 326°C. Downstream of the reactor, solids were separated from the HTL biocrude/aqueous stream by settling and filtration. Periodically, the solids were removed from the HTL system as a slurry and larger aggregates. The collected solids were then dried at 105°C and used as SCM in this study.

Table 1. Feed and yield in HTL process.

Feed composition		HTL run parameters		Mass yield (dry, normalized)	
Ash, wt%	44.8%	Temperature, °C	326	Biocrude yield	20%
Carbohydrate, wt%	45.0%	Pressure, MPa	19.6	Solid yield	14%
Fat, wt%	0.0%	Flow rate, L/h	2.3	Gas yield	28%
Protein, wt%	10.2%	Residence time, minutes	14	Aqueous yield	38%

Elemental analysis: To quantify the contents of ash and char in the algal biochar, the carbon, hydrogen, nitrogen, oxygen, and sulfur contents in the algal biochar were assessed following ASTM standards (D5373, D5291, D4239, D1552). Moisture content was gravimetrically determined by drying for 24 h at temperature of 105°C until mass loss ceased. Following moisture content measurement, ash content was determined gravimetrically by ramping to 750°C with 2° per min in a furnace.

Metal analysis: The objective is to determine the concentration and types of metals present. This is essential for assessing the biochar's suitability for various application, its potential environmental impact, and its effectiveness in process such as carbon sequestration and pollutant removal. Inductively coupled plasma (ICP)-optical emission spectrometry (OES) was conducted by using a PerkinElmer 7300DV OES instrument. This analysis utilized a customized approach based on ASTM D7692-11 standards. It entailed treating the samples with nitric/hydrofluoric acid followed by boric acid digestion to ensure the thorough dissolution of silica content. The HTL solid wastes were grinded by spice mill into powder sample for analysis. The metal compositions in HTL solid wastes are analyzed. The presence of other metals was also scanned but were below their respective detection limits.

Our cement mixture consists of commercially available type I/II portland cement, procured from Sakrete. The mineral composition of the portland cement is detailed in Table 2. Cement powder was fully mixed with silica fume (US silica, USA) with silica fume to cement ratio (s/c) of 3:7. Silica fume is a typical commercialized pozzolanic material. These samples with silica fume as admixture are used as control cement.

Table 2. Mineral compositions of type I/II portland cement.

Component	CaO	SiO_2	Al_2O_3	SO_3	Fe_2O_3	MgO	Na_2O	Others
Mass (%)	63.7	20.1	4.7	3.1	3.5	0.7	0.5	3.7
C_3S*		C_2S*		C_3A*		C_4AF*		Others
53		18		7		11		11

* Cement chemistry notation: S = SiO_2, A = Al_2O_3, C = CaO, F = Fe_2O_3.

Sample preparation. Table 3 shows the mixture of cement composites. Algal biochar powder was premixed with cement powder at biochar to cement ratio (b/c) of 3:7 and 1:7 separately. Next, deionized water was prepared separately in a plastic beaker, with a speed mixer operating at 300 rpm. The mixed biochar-cement powder was quickly poured into the beaker with deionized water to produce pastes, which were further homogeneously mixed at 800 rpm for another 18 minutes. Three different biochar-cement pastes were prepared at water-to-cement ratios (w/c) of 0.54, 0.65 and 0.78, respectively. Superplasticizer (SP), 0.5 wt% of calcium lignosulfonate based on dry solids mass, was added to samples AC1, AC2, AC3 and AC4. Then, the well-mixed fresh pastes were cast into cylindrical plastic molds to create samples for different testing needs. The molds with 1-inch diameter and 2-inch height were used for compression tests, while those with 2-inch diameter and 1-inch thickness were used for tensile tests. The cast slurries underwent vibration on a vortex mixer to remove any macroscopic air bubbles. Subsequently, the freshly cast samples were transferred to a closed chamber with 100% humidity for curing. The samples were kept for a curing period of 7 and 33 days before demolding and testing. Following the same procedure, control cement samples with a water-to-cement ratio (w/c) of 0.54 and a silica fume-to-cement ratio (s/c) of 3:7 were prepared as reference points for comparison with the biochar-cement composites. Samples were labeled for differentiation: CC for control cement and AC1-4 for algal biochar-cement composites at different b/c and w/c.

The role of SCM on the strength of cement mixture is analyzed by comparing three samples: CC, AC1 and AC4. Following the single-variable rule, only the dosage or type of SCM differs among these three samples. Another key factor for the strength development of cement pastes is water-to-cement ratio (w/c) in the mixture. To optimize the water content in biochar-cement composites, the role of water is examined by comparing three samples, AC1, AC2 and AC3. With the other variables fixed, three w/c ratios are evaluated. Based on these logics of experimental design, the following discussion will focus on the roles of SCM type (silica fume vs. algal biochar), new SCM (algal biochar) concentration, and w/c ratio on cementitious materials hydration and strength development."

Table 3. Mixture of cement composites

	Cement(g)	Algal biochar(g)	Silica fume (g)	Water/cement ratio	SP (g)	Water(g)
CC	210	0	90	0.54	0	113.4
AC1	210	90	0	0.54	1.5	113.4
AC2	210	90	0	0.65	1.5	136.5
AC3	210	90	0	0.78	1.5	163.8
AC4	210	30	0	0.54	1.2	113.4

Compression test. The objective of measuring the compressive strength is to assess its ability to withstand axial loads without failure. This key performance metric is crucial for determining the suitability of cement for construction applications, ensuring structural integrity, and verifying compliance with industry standards and specifications. Compression testing was conducted on at least three samples from each mixture after 7 and 33 days of curing. This testing was carried out using a universal test frame (MTS 312.21) outfitted with a 5 kN load cell. The rod samples with 1 inch (2.54 cm) by 2 inch (5.08 cm) were compressed at a constant force rate of 2224 N/min. This loading rate is small enough to avoid the inertial impact on samples. A 10% reduction in load was set as termination criteria, adhering to the ASTM C39/C39M-15a

standard. Maximum compressive strength and Young's modulus are output directly from the controlling software. The calculation of maximum compressive strength and Young's modulus refers to ASTM C39/C39M-15a standard.

Tensile test. The objective of performing a tensile test is to evaluate its tensile strength and measure its ability to resist tension or pulling forces. The tensile strength is vital for understanding the cement's performance in scenarios where tensile stresses are present, for example in oil, gas, and geothermal wellbores. Brazilian tensile testing was conducted for each mixture on a minimum of 3 samples after 7 and 33 days of curing using the same testing apparatus as compression test. The disk samples with 2-inch (5.08 cm) diameter by 1-inch (2.54 cm) tall were loaded by a curved fixture at a force rate of 2224 N/min. The loading termination is set as 10% reduction of force. Tensile strength is derived from the force-displacement curve based on the equation in ASTM C496 standards.

BET analysis. The objective of BET analysis is to determine the specific surface area and porosity of cement sample. This information is crucial for understanding the surface area, which influence its reactivity, and gas/vapors adsorption capacity. The pore structure and surface area of CC and AC samples are analyzed by N_2 physisorption at 77 K with an automatic gas sorption system: Autosorb iQ Gas Sorption System from Quantachrome Instruments (A brand of Anton Paar). The samples were treated at ~45 °C in a vacuum oven for 2-32 hours, then degassed under vacuum at 45 ˚C for 15 hours using MasterPrep degasser (Quantachrome Instruments) before the N2 physisorption measurements. The surface area was determined using 5 points BET (Brunauer-Emmett-Teller) method from the adsorption data in the relative pressure range of 0.05−0.3. BJH (Barrett, Joyner & Halenda) method was used for pore size analysis.

X-ray diffraction (XRD). The objective of using XRD for cement is to identify and quantify its crystalline phases and compounds. This analysis helps in understanding the mineral composition and detecting any phase transformations. Powder X-ray diffraction was collected on cement samples. Cement samples were grinded into fine powder through No. 30 sieve (0.6 mm). The powder samples were then mounted on a zero-background silicon wafer holder and scanned using a Bruker D8 Advance diffractometer with a Cu-target. PXRD patterns were collected at tube power of 40mA and 40kV, over a scan range of 5-70 ° 2-theta, step size of 0.015 ° 2-theta, and step time 1 s. The PXRD patterns were analyzed using EVA 6.0 software to remove $K\alpha_2$ diffraction peaks and then perform phase identification using the International Centre for Diffraction Data, Powder Diffraction File, version 1999.

Optical microscopy analysis. The optical microscopy analysis examines the microstructure of cement, including the size, shape, and distribution of its phases. This analysis provides insight into the porosity, potential defects, and overall quality. Optical microscopy analysis was conducted with an Olympus BX53M BF/DF Transmitted/Reflected Light Microscope for detailed observation of both CC and AC samples. The samples were first carefully placed on the microscope stage. We then adjusted the microscope to operate in Bright Field (BF) mode. The reflected light system was employed to illuminate the samples from above. Images were processed with Mosaic 2.3.1 software using its Live Extended Depth of Field (EDF) function to capture all details of a sample in a single image by manual focus control. This setup was particularly effective in revealing the characteristics of the algae-modified cement samples compared to the control group.

Scanning Electron Microscopy (SEM) and Energy-Dispersive X-ray Spectroscopy (EDS). SEM provides high-resolution imaging of its surface morphology and microstructural features. SEM and EDS together offer a comprehensive understanding of the cement's structural and compositional qualities, which are crucial for evaluating its performance and durability. The specimens were visualized via SEM (JEOL JSM-IT200LA) at an accelerating voltage of 10 kV to get high-resolution microstructural characterization.

Equipped with a JEOL JED-2300 Dry silicon drift type EDS detector, detailed elemental distribution and phase composition were examined at an accelerating voltage of 20 kV. The SEM images of precursor powders are used to quantify the particle size distribution by ImageJ.

CO_2 absorption test. Each SCM powder weas placed in a 450-mL containers and sealed. The container was at atmospheric pressure (15psi absolute). A wireless CO_2 sensor (PASCO, USA) was used to monitor the CO_2 concentration in the sealed container. CO_2 was injected to the container until 9000 ppm was reached. Then the container was sealed from the CO_2 source and the CO_2 sensor monitored the concentration of CO_2 for 7 days.

Water adsorption test. The water adsorption capacity of algal biochar and silica fume was evaluated. Five grams of each SCM were mixed with water in conical tubes and centrifuged for 20 minutes. This separated the free water, leaving the wetted SCM at the bottom. The weight of the wetted SCM was recorded, and the retained water volume was calculated. The experiment was repeated three times for each SCM to ensure accuracy.

Reactivity and bound water tests. The cumulative heat of reaction of two SCMs (algal biochar and silica fume) were measured in an isothermal calorimeter (Calmetrix I-Cal 8000 HPC, Calmetrix, MA, USA) continuously until 7 days at 40°C. The R3 test follows the procedure in standard ASTM C1897 Method A. The tested paste mixtures were prepared by mixing 5 g of SCM, 15 g of $Ca(OH)_2$, 2.5g $CaCO_3$, and 27 g of Potassium solution (KOH, K_2SO_4). Chemicals were obtained from Sigma-Aldrich (St. Louis, MO, USA). In addition, bound water content was performed following ASTM C1897 Method B. The tested pastes and SCMs were dried at 40°C to remove free water, then they were dried in a furnace at 350°C to evaporate the bound water. The bound water content in paste composites and SCMs are denoted as $H_2O_{bound,\ composite}$ and $H_2O_{bound,\ SCM}$. Then, the bound water involved in pozzolanic reaction is the difference, $H_2O_{bound,\ corrected} = H_2O_{bound,\ composite} - 0.101 \times H_2O_{bound,SCM}$.

▪ Results and Discussion

Particle morphology of algal biochar and silica fume. The powder samples and their cement products are presented in Figure 1. The SEM images of powder samples are measured using ImageJ to determine the particle size distribution. The type I/II cement particles have a mean particle size of 2 um (see Figure 1g). The mean particle size of silica fume is about 1.3 um (see Figure 1h). The mean particle size of algal biochar is about 0.8 um (see Figure 1i). The finer particle size of algal biochar compared to silica fume is clear from this analysis. Some large particles in Figure 1c are agglomeration of fine particles due to high adsorption of water (see Figure 1f). Additional micrographs are shown in Figure S1. The color of cement samples also shows differences (see Figure 1j, k). The control cement is white, whereas the algal biochar-cement composites are color.

The water adsorption capability (free water) of algal biochar and silica fume are measured as 1.64 ml/g and 0.48 ml/g, respectively (see Figure S2) demonstrating a significantly higher water retention potentially due to particle size and chemical composition differences between the two SCMs.

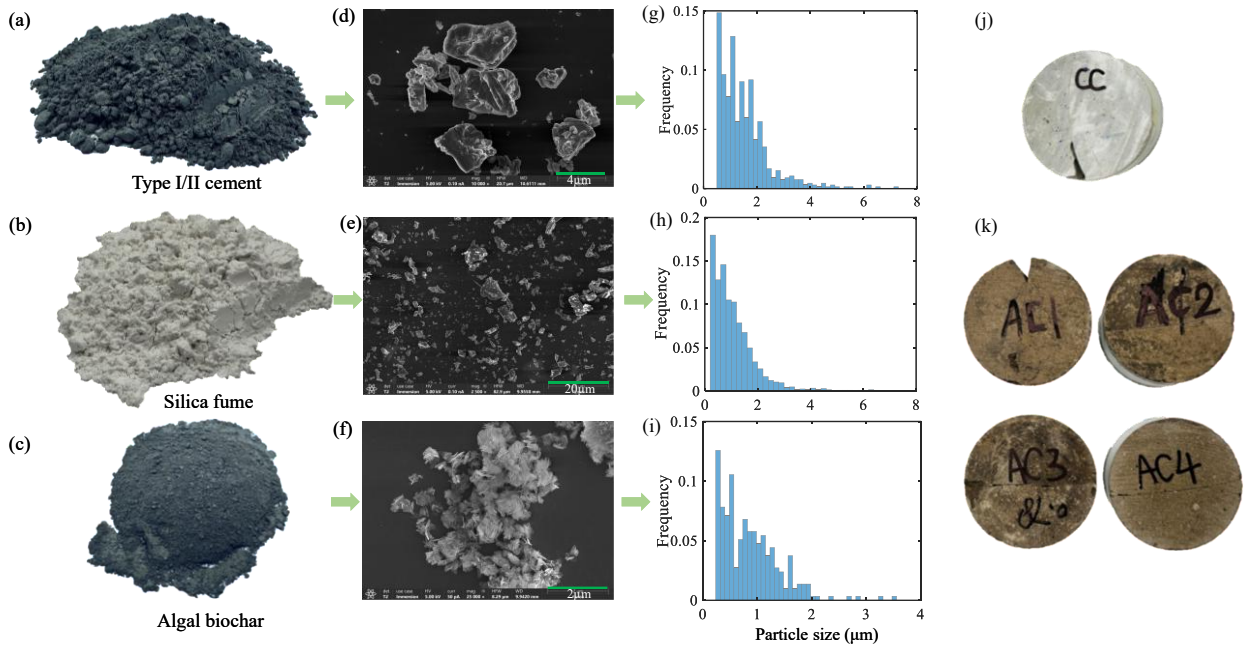

Figure 1. Powder characterization and sample presentations. Photographs of the (a) type I/II cement, (b) silica fume, (c) algal biochar. Particle morphology by SEM analysis: (d) type I/II cement, (e) silica fume, (f) algal biochar. Particle size distribution of three dry powders: (g) type I/II cement, (h) silica fume, (i) algal biochar. Photographs of the (j) control cement and (k) biochar-cement composites after tensile testing. Additional micrographs are shown in Figure S1.

Chemical reactivity of algal biochar and silica fume.

The reactivity of SCMs dictates their potential performance in cement. High reactivity generally indicates rapid strength gain, the formation of beneficial hydration products, and significant chemical changes. The R3 test is specifically employed to measure the chemical reactivity of algal biochar and silica fume, shown in Figure 2. The cumulative heat release over 7 days for algal biochar and silica fume is 76.2 J/g and 32.3 J/g, respectively, indicating higher chemical reactivity of algal biochar compared to silica fume. This is attributed to the large concentration of quartz in the silica fume, exhibiting significantly low reactivity, as observed in the control cement samples even after the sample was cured for 33 days as it is described in the next section. In contrast, the minerals in algal biochar are reactive and demonstrate high pozzolanic activity. In addition, the bound water content was measured in the two SCMs at curing time of 7 days and shown in Table 4. The bound water is distinct from free water and influences the reactivity and properties of SCMs. Higher bound water content in SCMs can indicate greater reactivity and portlandite consumption, hence higher pozzolanic activity. The corrected bound water of silica fume and algal biochar are 1.72% and 2.65%, respectively. This data is aligned well with the heat flow results from R3 test. It also infers the relatively low reactivity of the silica fume used in this study.

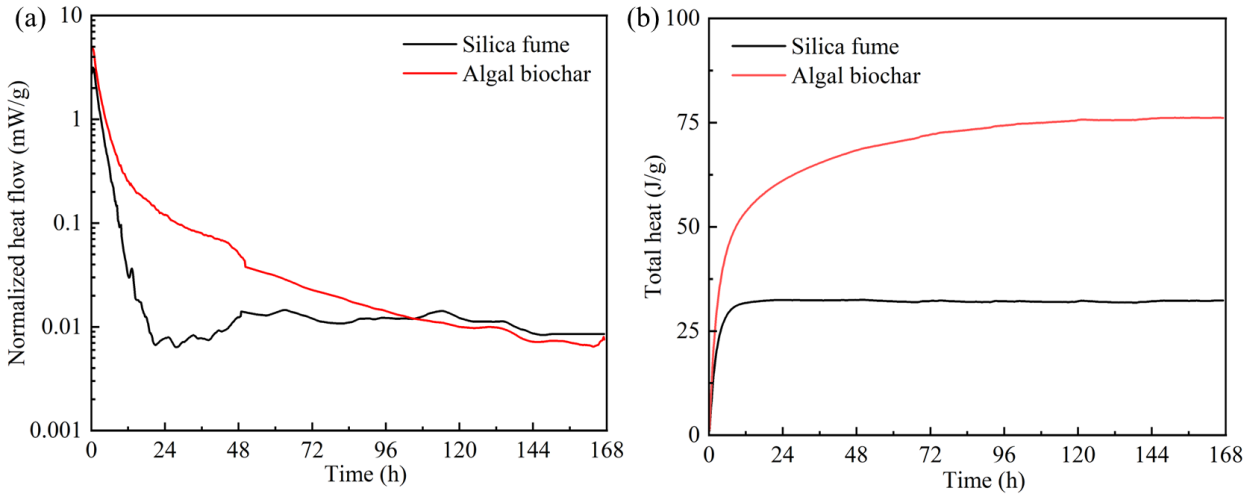

Figure 2. (a) The normalized heat flow and (b) cumulative heat release of two SCMs from isothermal calorimetry at 40°C for 7 days.

Table 4. Bound water content results for two SCMs at curing time of 7 days.

	$H_2O_{bound,\ composite}$ (%)	$H_2O_{bound,\ SCM}$ (%)	$H_2O_{bound,\ corrected}$ (%)
Silica fume	1.72 ± 0.04	0.03 ± 0.01	1.72 ± 0.04
Algal biochar	3.60 ± 0.06	9.38 ± 0.08	2.65 ± 0.05

Chemical compositions of algal biochar and cement. The algal biochar from HTL process is characterized and shown in Table 5. The char (organic part) accounts for 23 wt% and the ash (inorganic part) takes about 77 wt% in the solid waste. It has been demonstrated that the biochar has hindrance effect on the hydration and early strength enhancement of composites [25, 26]. It is found that algae possess functional groups such as -COOH and -OH that exhibit potential for retarding the nucleation and growth of hydration products in early stage hydration process [26]. Functional groups have been found to survive at reaction temperature of up to 500°C during the pyrolysis of seaweed[28]. In our HTL process, which operates at a reaction temperature of 326°C, these functional groups remain within the biochar. They act as retarder, slowing down the strength gain of cement paste. The influence on hydration kinetics of our algal biochar samples will be elaborated in next section. The C, H, N and S compositions are very similar to the characteristics of biochar produced from a range of algal species in literature [29]. Algal biochar has low H, C, and O content compared to biochar produced from lignocellulosic biomass in literature [30], in the opposite, it has higher ash content. The low C content and high ash content, compared to lignocellulosic biochar, are typical characteristics for algal biochar [29]. The H/C molar ratio and O/C molar ratio have been used to estimate the degree of carbonization and hydrophobicity in biochar respectively[31]. Compared with lignocellulosic biochar [30], the algal biochar has high H/C molar ratio (1.263) and high O/C molar ratio (0.83), indicating lower degree of carbonization and hydrophobicity and higher degree of polarity due to more aliphatic carbon structures, fewer aromatic carbon structures, and higher oxygen-containing functionalities. In general, H/C and O/C ratios of biochar reduce with the increase of HTL temperature which could be attributed to the loss of O and H [32, 33].

Table 5. HTL solid waste characterization: CHNOS and ash.

	Dry weight wt %					
Feedstock	C	H	N	S	O	ash
microalgae	16.575	1.7445	1.145	0.10121	18.346	76.98626

The elemental compositions of our algal biochar are presented in Table 6. The five most dominant elements are Al, Si, Na, Ca and Fe. The concentration of Al responds to a combination of original Al content in algae and the Al-based flocculant used during the algae harvesting process. There are also trace heavy elements (Cr, Ni, Cu and Zn) in the ash. There is also high content of hazardous waste elements (K and P). In the United States, materials listed on the U, P, K, and F lists are categorized as hazardous waste, as outlined in Title 40 of the Code of Federal Regulations (CFR) Part 261[3]. The valorization of ash as cementitious materials can safely store these hazardous elements in cement or concrete and convert disposal penalty to benefit of the HTL solid wastes. Conversely, the notable presence of alkali elements and alkaline earth metals (such as Na, K, Mg, Ca, etc.) detailed in Table 6 contributes to the alkalinity of algal biochar, with a pH typically hovering around 10, as observed through the analysis of various algal biochar samples[29]. This inherent alkalinity heightens the attraction towards acidic CO_2, resulting in an augmented adsorption capacity for CO_2[34, 35]. Consequently, these distinctive characteristics of algal biochar facilitate the chemical adsorption of acidic CO_2, leading to the formation of bicarbonates and carbonates.

Table 6. Inorganic elements in HTL solid waste.

Element	Al	Ba	Ca	Cr	Cu	Fe	K	Mg
Concentration(ppm)	87,000	130	14,000	670	51	11,000	6,300	2,500
Mn	Na	Ni	P	Sr	Zn	Si	Ti	S
930	27,000	60	5,400	50	67	79,000	1,800	1,000

The minerals identified by XRD analysis on algal biochar-cement composites are listed in Table 7, together with XRD patterns of control cement (cement: silica fume 70:30) and algal biochar. The associated phase signals are presented in Figure 3a. The dominant minerals are silicon oxide, ettringite [$Ca_6Al_2(SO_4)_3(OH)_{12}\cdot 26H_2O$], boehmite [AlO(OH)], eugsterite [$Na_4Ca(SO_4)_3\cdot 2H_2O$], hillebrandite [$Ca_2(SiO_3)(OH)_2$], and analcime [$NaAl(Si_2O_6)$]. It is remarkable to notice the high content of silica (SiO2) (45.8%) and boehmite [AlO(OH)] (29.1%) in inorganic ash in Table 7. Considering that 77 wt% of the algal biochar is inorganic, the silica and boehmite accounts for 35.3 wt% and 22.4 wt% of the algal biochar. This brings a value of aluminum and silicon element based on XRD analysis of 10 wt% and 16.5 wt% which is in the order of magnitude of the value attained by elemental analysis of the algal solids via ICP-OES (8.7wt% for Al and 7.9wt% for Si in Table 6). In contrast, the silica and boehmite accounts to 99.7 wt% and 0.05 wt% in silica fume. The different percentages of silica and boehmite in algal biochar and silica fume (used in control cement samples) affect hydration products and the resulting strength enhancement.

Table 7. Minerals in HTL solid wastes by XRD.

Minerals	Boehmite	Analcime	Eugsterite	Silicon oxide	Hillebrandite	Others
Phase intensity (%)	29.1	6.2	12.9	45.8	3.9	2.1

Both silica and alumina serve as exceptional pozzolanic additives. The addition of these two pozzolans has been reported to substantially enhance mechanical properties and durability, due to the synergistic effects of nucleation sites, filler effect, and pozzolanic reaction [36, 37]. During the early stage, cement hydration and pozzolanic reaction occur concurrently. However, cement hydration predominantly takes place during the initial curing period of the first 7 days. Beyond this period, the pozzolanic reaction becomes the dominant process and continues over a longer duration. Therefore, the measured content of portlandite results from the combined effects of cement hydration, which produces portlandite mainly in early age, and pozzolanic reaction, which consumes portlandite mainly in late age.

The pozzolanic additives (both silica and alumina) in algal biochar and silica fume are 57.7 wt% and almost 100 wt% respectively. Therefore, control cement with silica fume has higher degree of pozzolanic reaction than that of biochar-cement composites. The higher degree of pozzolanic reaction also indicates the finer microstructure of control cement due to the filler effect of pozzolanic activity. The difference of hydrated minerals and microstructures for control cement and biochar-cement composites will be elaborated in the next section.

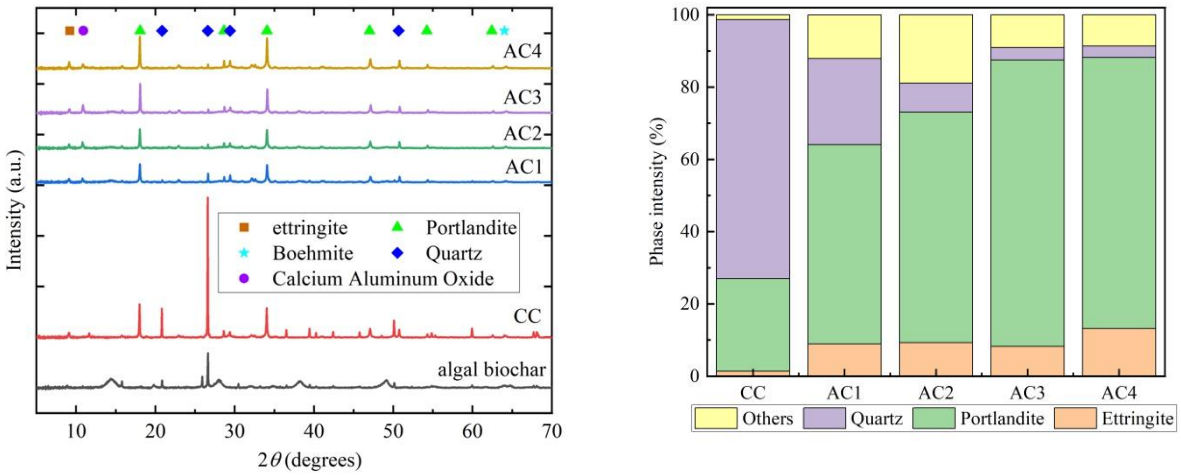

Figure 3. (a) XRD patterns of samples when cured for 33 days. (b) the phase intensity fraction of crystalline minerals in the different cement samples at early age. It is noted that the background signal has been subtracted in (a) to eliminate the effects of amorphous phases.

Mineral compositions of hydrated composites. The mineral compositions of algal biochar, control cement, and algal biochar-cement composites were investigated by using XRD. The C-S-H or C-A-S-H gel, the main hydration product together with portlandite, shows as an amorphous background that was subtracted. The mineral composition of algal biochar is listed separately in Table 7. The dominant minerals of other cement composites are exhibited in Figure 3a. It is noted that other trace minerals are not listed in the graph. All samples have been cured for 33 days, which can be regarded as the period dominated by the pozzolanic reaction. The signals for four biochar-cement composites (AC1, AC2, AC3 and AC4) are very similar and consistent, whereas the signal for control cement presents different 2θ peaks since the SCM used (silica fume) has a different composition. For the control cement, the main crystal minerals are silica and portlandite. There are also small concentrations of other minerals, such as ettringite, gypsum (2θ = 11.6°), and alite (2θ = 32.3°). The phases intensity for gypsum and alite is less than 1% and the residual of un-hydrated alite and gypsum may be attributed to buffering effect of hydration products on reactant

surface, which blocks further hydration of inner core minerals. The high content of portlandite and silica indicates that pozzolanic reactions at curing age of 33 days are yet to occur. As pozzolanic reaction advances, more silica and portlandite will be consumed and produce more C-S-H gel. The pozzolanic reaction is a long-term reaction.

The comparison of samples CC and AC1 with same w/c ratio in Figure 3b shows the lower content of portlandite and higher content of silica for control cement. The higher content of silica in control cement is attributed to the excessive silica fume after partial consumption with portlandite in pozzolanic reaction while the lower content of portlandite is associated to its pozzolanic reaction with silica. The comparison of cement composites with different w/c ratios (AC1, AC2 and AC3), shows that samples with higher w/c ratio present higher concentration of portlandite, which is consistent with the trend of plain cement [38]. This is attributed to (1) the high water-holding capacity of fine biochar (1.64 ml/g compared to 0.48 ml/g of silica fume), which reduces the availability of free mixing water and thus prevents the full hydration of the cement composite, and (2) a higher w/c ratio means more free water involved in hydration of cement mixture, leading to higher content of portlandite. This explanation is further supported by the comparison of samples AC1 and AC4 with same w/c ratio and different b/c ratio, where higher dosage of algal biochar reduces availability of free water and early formation of hydration products.

Microstructures of cement composites. The microstructures of control cement and biochar-cement composites were studied by nitrogen sorption technique. In addition to the solid hydration products, the microstructure of cement is shaped by a variety of voids generated through the ongoing physicochemical processes that occur during cement hydration and the pozzolanic reaction. Within cement samples, two primary categories of pores are observed: cement matrix pores, which encompass gel pores; capillary pores, formed because of the inherent volume alteration of portland cement during hydration. Per the pore size classification established by the International Union of Pure and Applied Chemistry (IUPAC), pores exceeding 50 nm in diameter are categorized as macropores, while those falling within the range of 2 to 50 nm are termed mesopores, and pores with diameters below 2 nm are designated as micropores[39]. Nitrogen adsorption technique is used to characterize the pores mainly in the mesopore range. The samples are first dried in an oven for 22 hours at 45°C, the mass loss is reported in Figure 4a. This mass loss corresponds to free water in capillary pores since the chemically bound water requires at least 400°C to release from portlandite. The similar mass loss for CC, AC1 and AC2 indicates the similar amount of pore water in the samples. The higher mass loss for AC3 indicates more free water since these samples were prepared with higher w/c ratio. The more mixing water used, the more water is released, resulting in occupation of additional voids. This, in turn, degrades the strength of cement composites, even though a small fraction of this excess water is then useful for late-age hydration and for pozzolanic reactions. The mass loss comparison for CC and AC4 indicates the more water absorption in pozzolanic reaction with silica fume as additive since higher content of pozzolan in control cement. This water consumption together with the higher water to dry mass ratio are the reason for higher mas loss associated to free water evaporation. Therefore, in terms of free water loss, a w/c ratio of 0.54 (sample AC1) is preferred since less free water is present after curing, reducing the pore volume as shown in Figure 4b. Sample AC1 also shows a bimodal distribution of pores, with smaller pore sizes (Figure 4d) compared to the other algal biochar-cement samples and even smaller than those in sample CC.

In terms of CO_2 storage capacity, algal biochar contributes about 16 wt% of stored biogenic and anthropogenic carbon, as evidenced by the carbon content observed in elemental analysis from Table 3. This immobilized carbon is subsequently stored within the cement composites. In addition, the microstructure and pore connectivity of cement composites largely determine the CO_2 physisorption capacity. The CO_2 capture potential of algal biochar, particularly with micropores measuring less than 1

nm in diameter[40], is expected to be significantly higher. This anticipation arises from the fact that narrow micropores closely approximate the dynamic diameter of a CO_2 molecule (0.364 nm), thus exerting a stronger attraction to CO_2. This enhanced affinity results from the overlapping adsorption forces and potential fields emanating from neighboring pore walls[41]. Micropores less than 1nm cannot be detected with this instrument, even though the dynamic diameter of infiltration gas N_2 is smaller (0.33 nm). Previous research has indicated that the specific surface area is a critical characteristic of biochar in CO_2 adsorption. Adsorbents possessing a large surface area tend to exhibit a higher capacity for CO_2 capture[42]. The larger surface area provides more active sites for CO2 adsorption through physical adsorption. BET is the most common method used to measure the surface area of porous materials. Y. Mochizuki et al[43]predicts that the mass of CO2 adsorbed tend to increase approximately linearly with an increase in specific surface area in porous carbon materials, indicating that surface area is an important factor influencing CO2 adsorption performance. The BET surface area of AC1 is 31% larger than that of CC sample, anticipating a 31% higher CO2 storage capacity from CO2 physisorption. Additionally, the algal biochar in samples AC1 through AC4 already contains about of 16 wt% of anthropogenic CO_2 stored. It is noted that besides the CO_2 physisorption, the above-mentioned alkaline elements and functional groups in algal biochar brings extra CO_2 capture capacity from CO_2 chemisorption[44]. The surface area comparison of samples AC1, AC2 and AC3 indicates the higher CO_2 capture capacity with higher w/c ratio, though at the cost of reduction in mechanical strength as it will be shown in the next section. Similarly, the surface area comparison of samples AC1 and AC4 infers the higher CO_2 capture capacity with higher b/c ratio. Nevertheless, the surface area of both algal biochar and silica fume-based composite is low compared to other porous materials, like activated carbon. The BET surface area of ordinary Portland cement is between 1.5-1.8 m^2/g[45], while some agricultural biochar has high surface area, over 200 m^2/g[30].

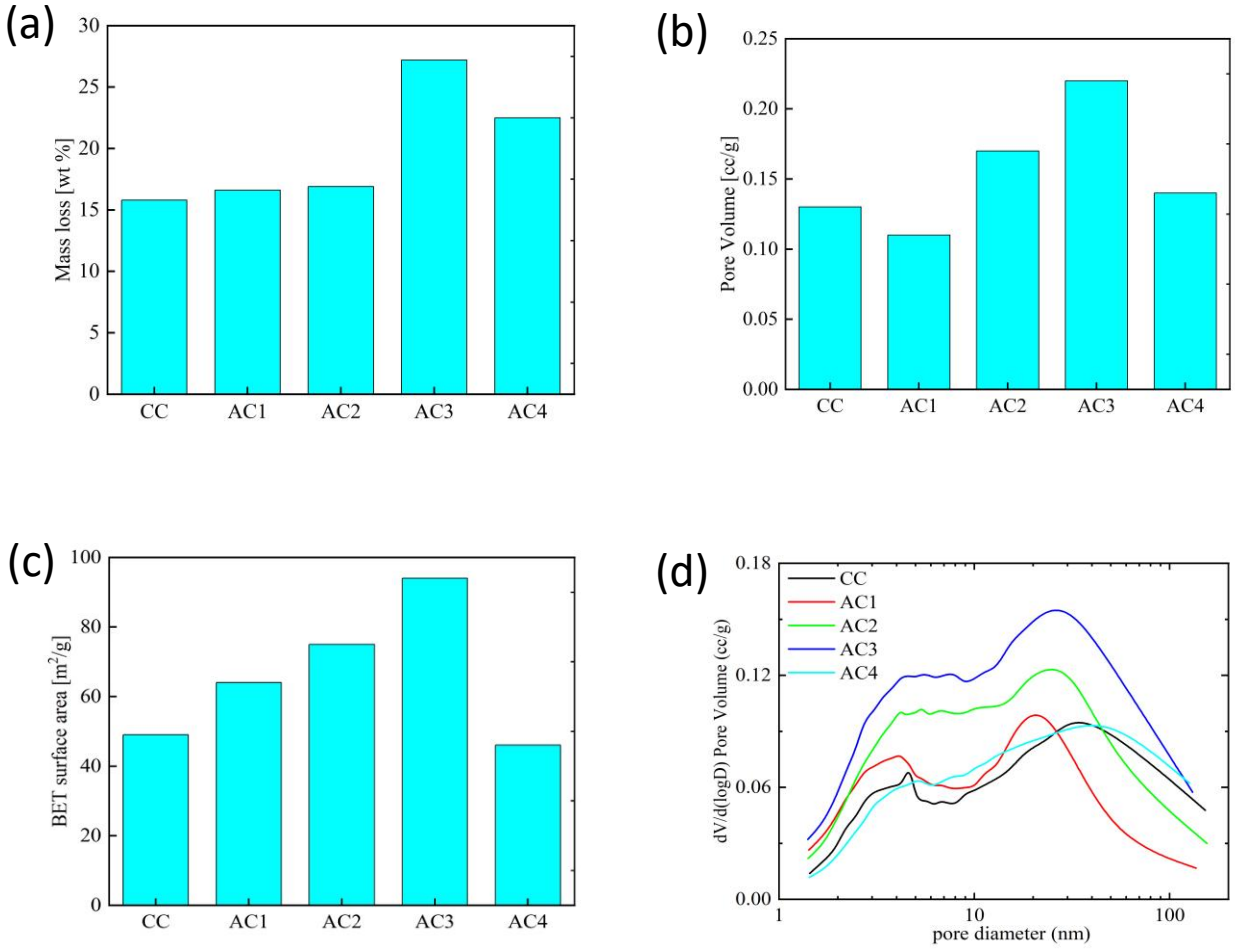

Figure 4. (a) mass loss of tested composite samples in preparation for BET measurement at 45°C for 22h. (b) the measured pore volume of samples. (c) the BET surface area. (d) the mesopore size distribution in the samples. The samples are cured for 30 days.

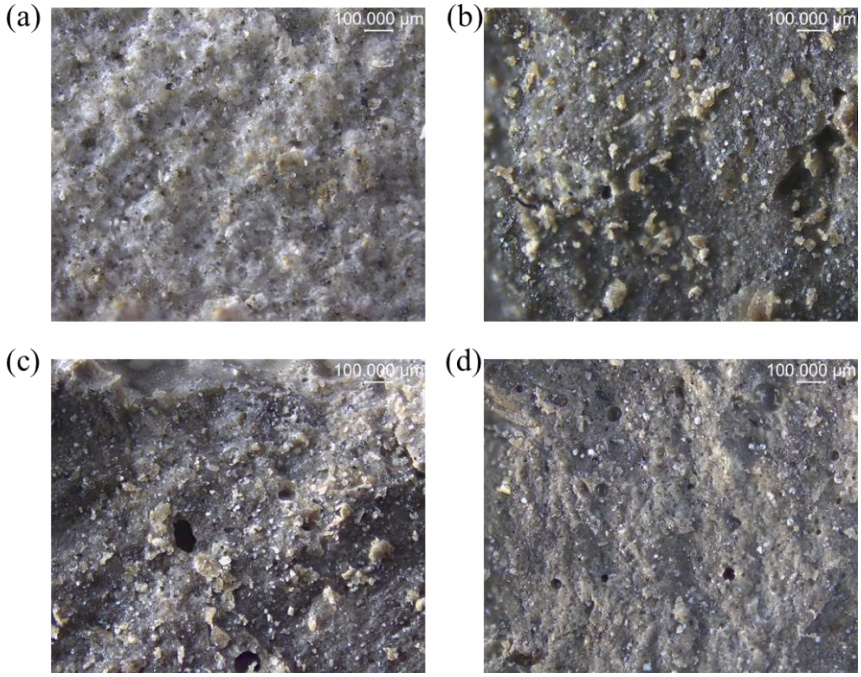

Figure 5. Surface morphology of cement samples using optical microscopy: (a) CC, (b) AC1, (c) AC2 and (d) AC3.

Porosity was also examined by optical microscopy. The samples were broken by a hammer and the cracked surface was observed without any surface treatment. The rough surface morphology of four samples (CC, AC1, AC2 and AC3) are exhibited in Figure 5. The surface in Figure 5a is very dense without visible pores and cracks. It indicates the dense structure of the control cement and uniform dispersion of the minerals in hardened samples. In contrast, the dark yellow agglomerates in Figure 5b and 5c are heterogeneously distributed on the surface. They would correspond to the organic fraction of algal biochar that didn't undergo hydration or pozzolanic reactions. The small pores in the micrographs represent the porous structure of algal biochar-cement composites. These pores become more noticeable and frequent with higher w/c ratio from Figure 5c and 5d. The pores left behind by water evaporation in Figure 4d are clearly shown due to excessive water content in samples. The pore sizes are extracted from microscopy images. The pore size distribution in algal biochar-cement composites is presented in Figure S3. The mean pore sizes for samples (AC1, AC2, AC3 and AC4) are 4.6 um, 15.2 um, 33.6 um, and 11.8 um, respectively.

The morphology of both algal biochar powder and hardened cement composites are exhibited in Figure 6. From Figure 6a and 6e, we observe that the algal biochar looks fuzzy and presents nano-scale particle size. The agglomeration of biochar powder in Figure 6a is attributed to fast absorption of atmospheric water vapor in sample preparation. The high surface area and agglomeration corroborate the high affinity of water absorption in mixing of algal biochar-cement slurry. In contrast, the average particle size for type I/II portland cement is about 2 μm and it is about 1.3 μm for silica fume based on our measurement in Figure 1. It is inferred that algal biochar with tiny particle size will show greater filler effect than silica fume. Figure 6b and 6f shows representative hydrated products for control cement, i.e., needle-like ettringite, hexagon-shaped portlandite, amorphous C-A-S-H paste. It is observed that the C-A-S-H paste binds the uniformly distributed portlandite crystal and there are no discernible defects in zone of interest. However, the macropores are captured for sample AC1 in Figure 6c, which will impair the strength of hydrated product. The C-A-S-H gel presents different morphology. C-A-S-H gel usually presents significant

morphological diversity with different C/S ratios [46]. The morphology of C-A-S-H in samples AC1 and AC3 are similar, but different from that in sample CC. The C-A-S-H gel in sample AC3 presents foil-like morphology as shown in Figure 6h.

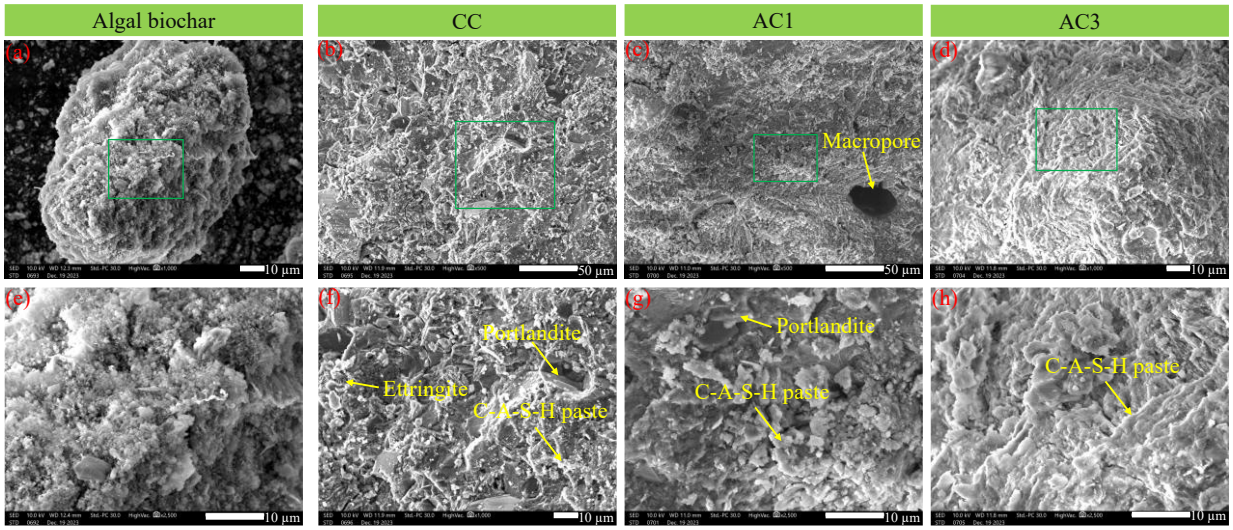

Figure 6. SEM micrographs of algal biochar powder and cement composites: (a) and (e) algal biochar; (b) and (f) CC composite; (c) and (g) AC1 composite; (d) and (h) AC3 composite. The figures in second row are the higher magnification of marked zone in first row.

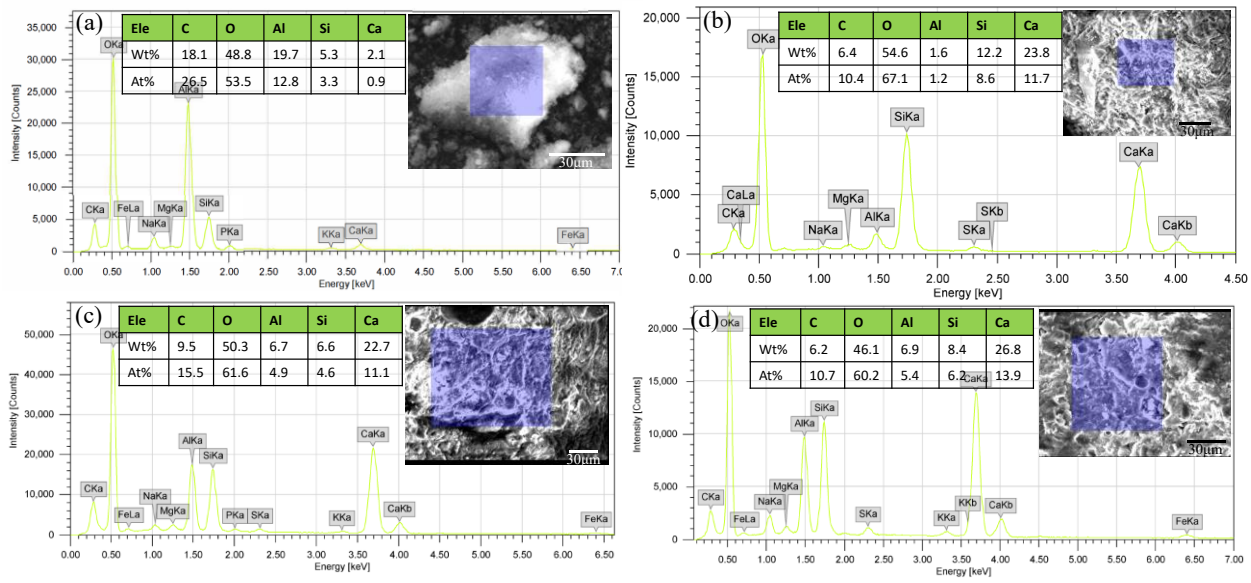

Figure 7. The element identification by EDS technique for (a) algal biochar, (b) CC, (c) AC1, and (d) AC3. The investigated region is marked by light blue color in the inset. The dominant elements are summarized as weight percent and atomic percent. The other trace elements are not presented.

The elemental distribution for four samples (algal biochar, CC, AC1 andAC3) is identified by EDS analysis, as shown in Figure 7. The raw data of intensity and excited energy is presented, along with identified elements as labels. The dominant elements are summarized in the table as inset in each graph. It is noted

that the identified elements belong to both amorphous and crystalline minerals in hardened cement samples, as compared to the mere identification of crystalline minerals by XRD technique. Therefore, C-A-S-H gel, the main hydration product, is also accounted for in elemental summary provided by EDS, offering greater insight into the hydration process. The elemental composition in algal biochar in Figure 7a indicates the high fraction of organic matter and the dominance of alumina in inorganic minerals. It is consistent with the data in Table 5 and 6, from different resources of characterization. The sample CC in Figure 7b presents C element, which may be attributed to carbonation of samples exposed to atmosphere. Likewise, carbonation also contributes to the presence of C element in samples AC1 and AC3. It is interesting to compare the composition of C-A-S-H gel between cement samples. C-S-H stands as the primary hydration product of hydrated portland cement, playing a pivotal role in determining the strength of portland cement-based concrete. Its composition varies and is frequently characterized by its average Ca/Si ratio and water content. Upon hydration of pure portland cement, a C-S-H phase with a Ca/Si ratio of approximately 1.7 is typically formed.[47] However, as the substitution with SCMs increases, this ratio tends to decrease. Consequently, the Ca/Si ratio of the C-S-H varies within a range of approximately 0.67 to 2.0[48, 49]. For sample CC with silica fume as SCM, the Ca/Si ratio is 1.36. With higher fraction of alumina in algal biochar, the hydrated product for algal biochar-cement composites becomes C-A-S-H gel. The Al/Si ratio can indicate the fraction of alumina preferred gel in hydrated product. The Al/Si ratios for samples CC, AC1 and AC3 are 0.14, 1.06 and 0.86, respectively. Therefore, they are higher fraction of alumina preferred gel in hardened samples. The overall Ca/(Al+Si) ratio for samples CC, AC1 and AC3 are 1.20, 1.17, 1.21, respectively, which is very similar.

Compressive strength of cement composites. We assess the dependence of the compressive strength on different w/c ratio and b/c through quasi-static compression test at different curing times, as shown in Figure 8. As anticipated, high dosage of mixing water results in reduction of the compressive strength of the algal biochar-cement composites. Specifically, high content of mixing water for samples AC2 and AC3 results in high pore volume and hence reduces the strength of composites, compared to the sample AC1. The fine algal biochar present in composites retains a portion of the mixing water during the early stages, resulting in a lower effective w/c and subsequent densification of the mortar. As time progresses, the retaining water in the pores is gradually released, aiding in improved moisture redistribution, and supporting the pozzolanic reaction of the generated calcium hydroxide. This is demonstrated by the compressive strength increase in all four biochar-cement composites (AC1, AC2, AC3 and AC4) by 64%, 64%, 13% and 5% respectively, with the compressive strength of sample AC1 matching that of sample CC at 33 days. In contrast, the commercial silica fume-based cement (CC) shows high early strength (7 days) that only increases by 10% at curing age of 33 days. The difference of initial strength and strength increase over time for samples AC1 and CC are attributed to the different availability of mixing water for cement hydration and pozzolanic reaction. For sample CC, mixing water is mainly used in cement hydration resulting in high early strength, the remaining water participates then in pozzolanic reactions, with a slow increase in strength. On the contrary, partial content of mixing water is retained by algal biochar and released slowly with time, resulting in slower hydration rates followed by pozzolanic reactions. The initial strength is low, but the strength enhancement is significant. Therefore, the algal biochar-based composites impart low early strength and long-term high strength compared to silica fume-based cement. It is also important to note that sample AC4 has 1/3 the concentration of algal biochar or pozzolanic material that AC1 has. Therefore, the pozzolanic activity responsible for strength development after 7 days, by converting CH into CSH and CASH, is significantly lower in AC4 and, as a result, AC4's strength is slightly improved from 7 to 33 days as compared to AC1.

The static modulus of elasticity is extracted from load-displacement curve before peak-load under compressive loading. The comparison of Young's modulus in Figure 8c has the same trend with that of

compressive strength in Figure 8a. The Young's modulus of control cement is highest at early age of cement hydration. However, in the period of pozzolanic reaction, the control cement attains only a 2% increase, compared to 71%, 74%, 12% and 90% increments of Young's modulus from 7-day to 33-day curing for algal biochar-based samples (AC1, AC2, AC3 and AC4) respectively. The underlying mechanism is the different effects of SCMs on cement hydration and pozzolanic reaction.

The ultimate value of compressive strength and Young's modulus are important for construction materials. With w/c ratio of 0.54 and b/c ratio of 0.43, cement composites with algal biochar exhibit comparable compressive strength and Young's modulus after a curing period of 33 days, to that of control cement with commercial silica fume. It is anticipated that the ultimate strength and modulus of biochar-based composites will be higher in the long term.

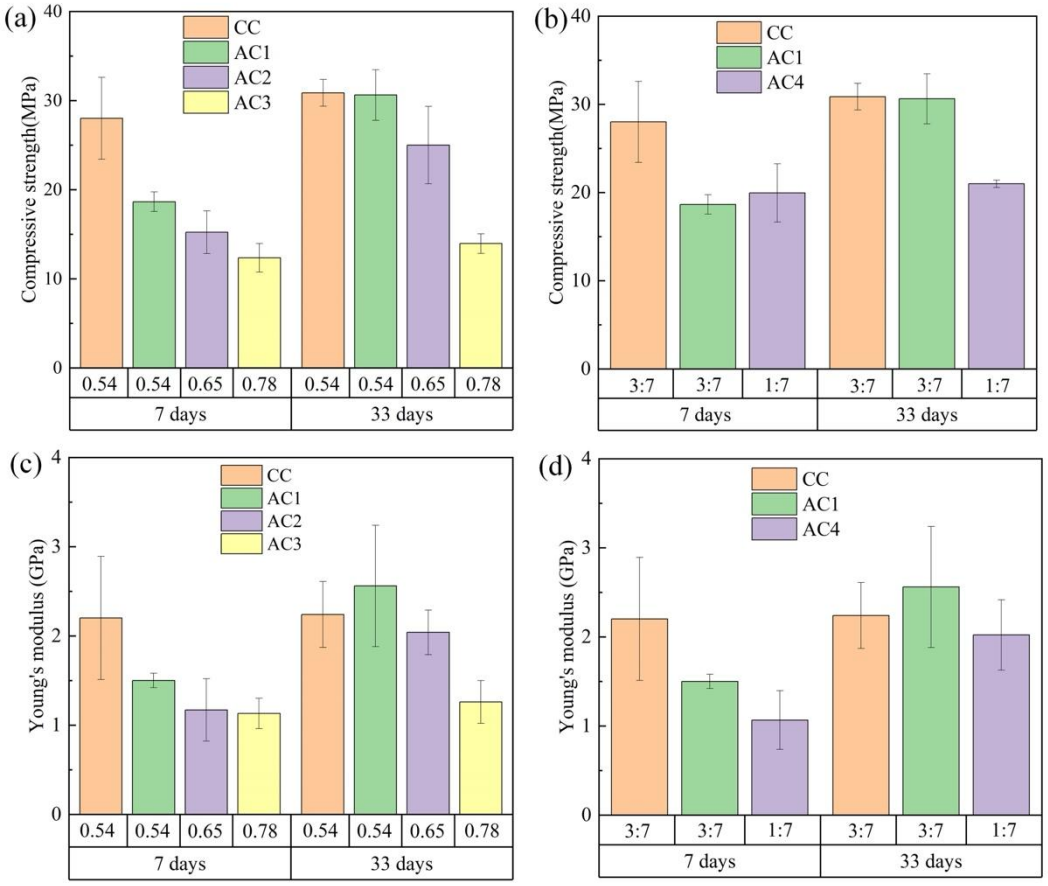

Figure 8. Compressive strength of different cement composites: (a) with different w/c ratio, and (b) different b/c or s/c ratio. Young's Modulus of different cement composites: (c) with different w/c ratio, and (d) different b/c or s/c ratio. Results are for 7-day and 33-day curing times.

Tensile strength of cement composites. The average tensile strength and its standard deviation are summarized in Figure 9. The tensile strength is the maximum tension the samples can withstand without breaking. The micropores and mesopores in cement samples are defects for loading bearing of tension. Pores and microcracks will grow and coalesce into macrocracks under tensile loading. However, these defects will close under compressive loading if they are not aligned with the loading direction. The different response to loading causes high compressive strength and low tensile strength of general cement samples.

The comparison of tensile strength presents a similar trend to that of compressive strength and Young's modulus, where tensile strength increases over time due to ongoing hydration and, subsequently, pozzolanic reactions. However, sample CC has the highest tensile strength compared to AC1, AC2, and AC3, regardless of aging time. The changes of tensile strength for samples CC, AC1, AC2, AC3 and AC4 are 152%, 57%, -8%, 41% and 15%, respectively. The low tensile strength of biochar-cement composites is attributed to the presence of macropores, particularly in the algal biochar-cements with higher w/c ratio, as seen in Figure 5. It is hypothesized that the micro-pores of algal biochar-cement paste introduce many weaker points compared to the bulk cement paste. These weak zones act as defects affecting the tensile strength of cement sample. On the other hand, pozzolanic products have filler effects that help occlude voids in cement samples. The comparatively higher increment in tensile strength for the control samples indicates the strong filling effect of silica fume-based pozzolanic reaction, which results in lower pore volume. Therefore, the tensile strength of algal biochar-based cement composites is lower than that of control cement with commercial silica fume. Further studies, including long-term (months) tensile strength evolution of samples like AC1, are required to determine if algal biochar can be used as a waste-based alternative to commercial pozzolans in cement.

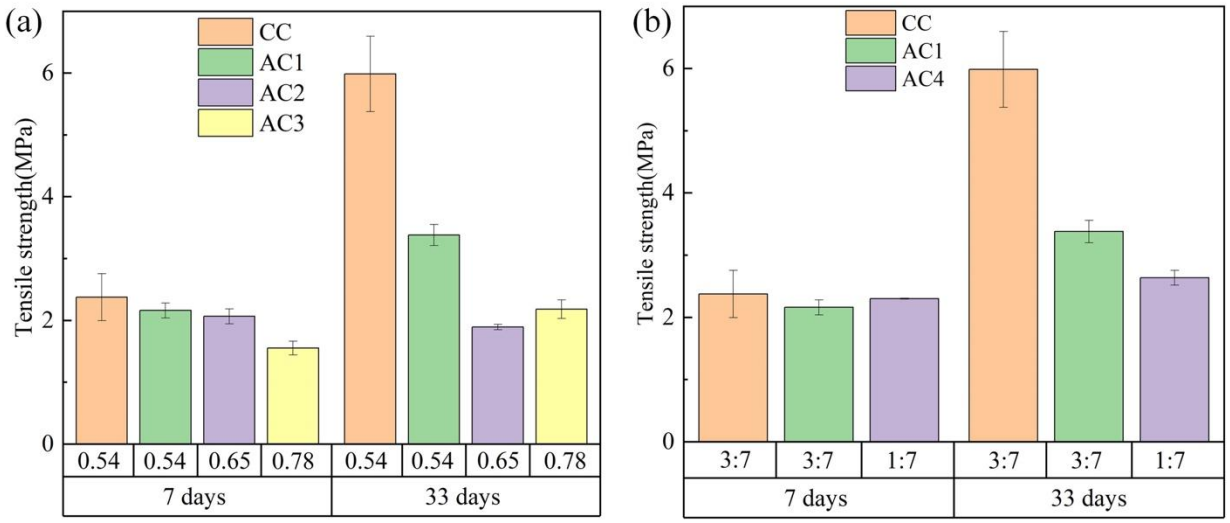

Figure 9. Indirect tensile strength of different cement composites: (a) with different w/c ratio, and (b) different b/c or s/c ratio, at both 7-day and 33-day curing times.

Effects on hydration and pozzolanic reaction. This section summarizes the effects of two SCMs, silica fume and algal biochar, on the cement hydration and pozzolanic reaction, as illustrated in Figure 10. Among the precursors, cement has the largest particle size, whereas algal biochar has the smallest. During the mixing stage, silica fume mixes well with cement, while the algal biochar tends to agglomerate and retain free water. This results in less free water for cement hydration for algal biochar-cement samples. The outer surface of cement particle hydrates to form hydration products, specifically C-S-H and portlandite. Due to limited accessibility of free water during hydration, the reaction for algal biochar-cement composites is slower compared to silica fume-cement composites. In the long-term, the retained water in algal biochar gradually releases, facilitating the pozzolanic reaction. Consequently, the un-hydrated cement core progressively reacts to form C-S-H at the expense of portlandite consumption.

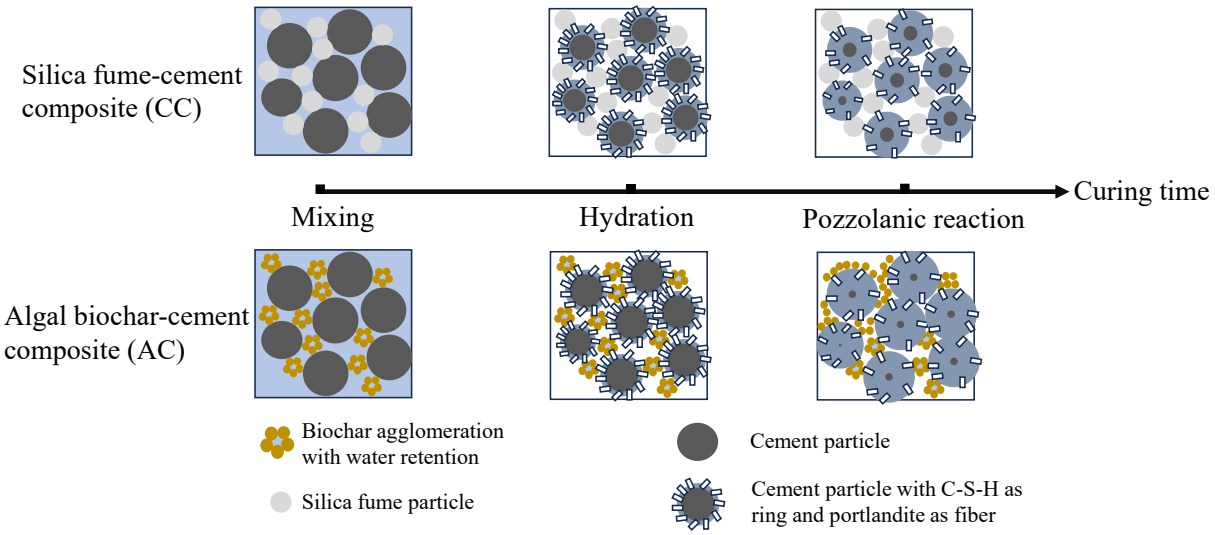

Figure 10. Schematic illustration of the effect of two SCMs (silica fume and algal biochar) on the cement hydration and pozzolanic reaction.

Life cycle analysis of cement composites. The environmental impact of two formulations based on algal biochar and silica fume is assessed through life cycle analysis (LCA). The LCA adheres to the international standard series ISO 14040. The primary goal is to evaluate the environmental impact of two cement formulations with different SCMs. The functional unit is the production of one cubic meter of cement composite. Due to the uncertainty of use, maintenance, and disposal, this analysis mainly focuses on the cradle-to-gate stage, which includes the extraction of raw materials, transportation to the manufacturing facility, and the manufacturing process itself. A schematic representation of the system boundary is shown in Figure 11. As a potential SCM in cement, the embodied carbon of algal biochar is calculated from the growth of algae to the production process. The embodied carbon of other components is readily extracted from the environmental product declarations (EPDs) provided by manufacturers. The life cycle inventory analysis is presented in the supporting information. The LCA results, displayed in Table 8, show comparable embodied carbon for the two cement composites. It is noted that this analysis is only applicable to cement products, as it does not account for carbon capture during the gate-to-grave stage. Furthermore, it is noteworthy to mention that the carbon absorption ability of algal biochar in the cement composite will be significantly higher as shown in Figure S4. The small particle size and carbon content of algal biochar facilitate anthropogenic carbon capture which will then be converted to calcium carbonate. Therefore, the algal biochar-based cement composite is anticipated to absorb more carbon dioxide during its service cycle (~70 years).

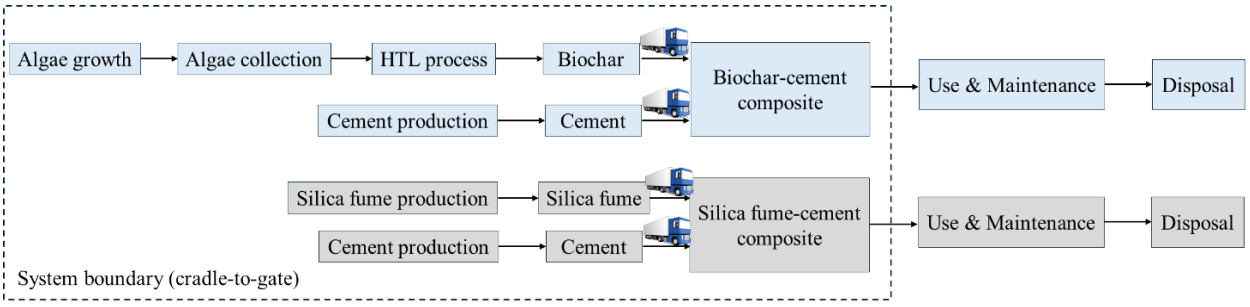

617 Figure 11. Schematic representation of the system boundary (cradle-to-gate) in LCA.

618 Table 8. Embodied carbon breakdown for cement composites (per cubic meter)

Algal biochar-cement composite (3:7)		Silica fume-cement composite (3:7)	
Item	Embodied carbon (kg CO_2 eq.)	Item	Embodied carbon (kg CO_2 eq.)
Cement	715.7	Cement	718.6
Algal biochar	34.3	Silica fume	16.3
Water	0.07	Water	0.07
Transportation	5.07	Transportation	5.08
SP	9.79		
Total	764.93	Total	740.05

619 Note: calculation based on formulation of CC and AC1 in Table 3.

620

621 **Cost-effective significance.** Microalgae are a diverse group of aquatic organisms that are mainly collected
622 from lakes and oceans. Currently, over 200 microalgae species are used globally and the total production
623 reaches over 30 million tons in USA[50]. Besides the positive environmental impact of using algae-derived
624 cement composites, another advantage of algal biochar-based admixture lies in its cost-effectiveness. As
625 waste products from biofuel production, the disposal of HTL solid waste becomes a penalty for the value
626 of biofuel production. The national average solid waste disposal is at cost of $55 per ton[15]. Its use in
627 cementitious materials brings credit to the solid waste and the biofuel production. Additionally, as
628 admixture in cementitious materials, its use can relieve the shortage of SCMs (e.g., silica fume) used as
629 pozzolanic materials in cement. Algae-derived admixtures bring to zero the increasing cost of commercial
630 SCMs and promote the adoption and commercialization of carbon negative waste-derived SCMs in the
631 concrete industry. In addition to the carbon storing capability, algal-derived biochar can potentially equip
632 cementitious materials with the capacity to immobilize heavy metals from wastewater in concrete
633 infrastructure. The economic comparison of two SCMs are presented in Table 9.

634 Table 9. Economic comparison of two SCMs in this study.

SCM	Unit price ($/kg)	Note
Algal biochar	0.0532	Based on price of soil remediation agent
Silica fume	0.5	Market price from manufacturer

635

636 **Conclusion**

637 This study explores the potential valorization as admixture in cementitious materials of solid waste from
638 the HTL conversion of algae to biofuels. The algae-derived solid wastes are characterized in terms of
639 elemental composition and minerals. The algae-derived solid wastes (algal biochar) are added into cement
640 at different w/c ratio and b/c ratio. Based on the experimental results, the following conclusions can be
641 drawn:

642 (1) The addition of algae-derived solid waste at a 3:7 ratio with cement presents comparable
643 compressive strength and Young's modulus to the reference (commercial) cement composites
644 (silica fume:cement 3:7) after 33-day curing. The reduction of w/c ratio increases the mechanical
645 performance of cement composites, making it comparable to commercial pozzolan-cement product.
646 The best w/c ratio based on strength in the investigated w/c ratio range is 0.54.

(2) The tensile strength of algal biochar-cement composites is comparable to that of the reference cement in the first 7-days (hydration reaction). However, the strength evolves at lower rates between 7-day and 33-day of curing (pozzolan reaction), and the tensile strength of algal biochar-cement composites is only 57% of that of the reference cement after 33 days.
(3) Algal biochar in cement admixture holds up part of mixing water and reduce the available/effective free water content in the mortar mix. This hinders the hydration and pozzolanic reaction in biochar-cement composites and retards the evolution of strength. The addition of an accelerator may improve the tensile strength of algal biochar-based cement composites, which will be reported in the follow-up publication.
(4) Algal biochar-based cement binders showed comparable embodied carbon as silica fume-based cement binders based on cradle-to-gate LCA.
(5) Algal biochar-based cement composites bring values for both biofuel production and cement application. The estimated unit price of algal biochar is 10 times lower than silica fume which represent another reason why these materials have significant potential as SCMs.

Supporting Information

The Supporting Information is available in a separate file:

SEM micrographs of type I/II cement, silica fume, and algal biochar; Comparison of water absorption for algal biochar and silica fume; Optical microscope image of biochar-cement samples; CO_2 absorption for algal biochar and silica fume; Life-cycle assessment for cement samples.

Acknowledgements

We gratefully acknowledge AECOM Technical Services Inc. for supporting this work by providing algae samples used for laboratory experiments.

This research received financial support from the U.S. Department of Energy (DOE), Office of Energy Efficiency and Renewable Energy, Bioenergy Technologies Office (BETO), and was conducted at the U.S. DOE's Pacific Northwest National Laboratory (PNNL) under contract DE-AC05-76RL01830. The work at PNNL was carried out within the framework of the WSU-PNNL Bioproducts Institute, a collaborative research initiative between Washington State University (WSU) and PNNL. The opinions expressed in this article do not necessarily reflect those of the U.S. DOE or the United States Government. The U.S. Government, its agencies, or any of their personnel do not provide any warranty, expressed or implied, nor do they assume any legal liability or responsibility for the accuracy, completeness, or usefulness of any information, apparatus, product, or process disclosed herein, nor do they assert that its use would not infringe privately owned rights.

Reference

(1) Toor, S. S.; Rosendahl, L.; Rudolf, A. Hydrothermal liquefaction of biomass: a review of subcritical water technologies. *Energy* **2011**, *36* (5), 2328-2342.
(2) Snowden-Swan, L. J.; Li, S.; Jiang, Y.; Thorson, M. R.; Schmidt, A. J.; Seiple, T. E.; Billing, J. M.; Santosa, D. M.; Hart, T. R.; Fox, S. P. *Wet waste hydrothermal liquefaction and biocrude upgrading to hydrocarbon fuels: 2021 state of technology*; Pacific Northwest National Lab.(PNNL), Richland, WA (United States), 2022.
(3) Middleton-Smith, L. A.; Zacher, A. H.; Blackwell, S.; Benemann, J.; Lundquist, T. Disposition of Solids from Hydrothermal Liquefaction of Biomass: Current Understanding, Research Gaps, and Opportunities. *Energy & Fuels* **2023**, *22* (37), 17301-17309.

(4) Cristina, G.; Camelin, E.; Garofalo, S. F.; Salomone, F.; Pugliese, M.; Gullino, M.; Tommasi, T.; Fino, D. Time-based evaluation of bioavailable phosphorus in a calcareous soil after the application of anaerobically digested sewage sludge. *Biomass Conversion and Biorefinery* **2022**, *12* (10), 4361-4373.
(5) Ponnusamy, V. K.; Nagappan, S.; Bhosale, R. R.; Lay, C.-H.; Nguyen, D. D.; Pugazhendhi, A.; Chang, S. W.; Kumar, G. Review on sustainable production of biochar through hydrothermal liquefaction: Physico-chemical properties and applications. *Bioresource technology* **2020**, *310*, 123414.
(6) Ovsyannikova, E.; Kruse, A.; Becker, G. C. Valorization of byproducts from hydrothermal liquefaction of sewage sludge and manure: the development of a struvite-producing unit for nutrient recovery. *Energy & Fuels* **2021**, *35* (11), 9408-9423.
(7) Gupta, S.; Kua, H. W.; Low, C. Y. Use of biochar as carbon sequestering additive in cement mortar. *Cement and concrete composites* **2018**, *87*, 110-129.
(8) Vassilev, S. V.; Vassileva, C. G.; Song, Y.-C.; Li, W.-Y.; Feng, J. Ash contents and ash-forming elements of biomass and their significance for solid biofuel combustion. *Fuel* **2017**, *208*, 377-409.
(9) Li, J.; Long, X.; Zhu, H.; Liu, Z.; Lu, X.; Zhang, D. Investigation into the fusibility of biomass ashes and their mineral phase transformations at elevated temperatures by using the HT-XRD technique. *Biomass and Bioenergy* **2023**, *173*, 106812.
(10) Azmi, M.; Ismail, N.; Rizamarhaiza, M.; Taib, H. Characterisation of silica derived from rice husk (Muar, Johor, Malaysia) decomposition at different temperatures. In *AIP Conference Proceedings*, 2016; AIP Publishing: Vol. 1756.
(11) Sachdeva, S.; Kumar, R.; Sahoo, P. K.; Nadda, A. K. Recent advances in biochar amendments for immobilization of heavy metals in an agricultural ecosystem: A systematic review. *Environmental Pollution* **2023**, *319*, 120937.
(12) Energy, D. o. *Pathways to commerical liftoff: low-carbon cement*; 2023.
(13) Energy, D. o. *Bioenergy Technologies Office 2020 R&D State of Technology*; 2020.
(14) Energy, D. o. *2016 Billion-Ton Report: Advancing Domestic Resources for a Thriving Bioeconomy*; 2016.
(15) *Analysis of Municipal Solid Waste Landfill Tipping Fees*; Environmental Reserach and Education Foundation, 2020. https://erefdn.org/product/analysis-msw-landfill-tipping-fees-2/ (accessed Dec, 2024).
(16) James, J.; Rao, M. S. Reactivity of rice husk ash. *Cement and concrete research* **1986**, *16* (3), 296-302.
(17) Choi, W. C.; Yun, H. D.; Lee, J. Y. Mechanical properties of mortar containing bio-char from pyrolysis. *Journal of the Korea institute for structural maintenance and inspection* **2012**, *16* (3), 67-74.
(18) FERRO, L. R. G. Nanoparticles from food waste: a “green” future for traditional building materials. In *Proceedings of the 9th International Conference on Fractur e Mechanics of Concrete and Concrete Structures*, 2016.
(19) Kang, S.; Jung, J.; Choe, J. K.; Ok, Y. S.; Choi, Y. Effect of biochar particle size on hydrophobic organic compound sorption kinetics: applicability of using representative size. *Science of the Total Environment* **2018**, *619*, 410-418.
(20) Ahmad, S.; Tulliani, J. M.; Ferro, G. A.; Khushnood, R. A.; Restuccia, L.; Jagdale, P. Crack path and fracture surface modifications in cement composites. *Frattura ed Integrità Strutturale* **2015**, *9* (34).
(21) Akinyemi, B. A.; Adesina, A. Recent advancements in the use of biochar for cementitious applications: A review. *Journal of Building Engineering* **2020**, *32*, 101705.
(22) Legan, M.; Gotvajn, A. Ž.; Zupan, K. Potential of biochar use in building materials. *Journal of Environmental Management* **2022**, *309*, 114704. DOI: https://doi.org/10.1016/j.jenvman.2022.114704.
(23) Hernández, E.; Cano-Barrita, P. d. J.; Torres-Acosta, A. Influence of cactus mucilage and marine brown algae extract on the compressive strength and durability of concrete. *Materiales de Construcción* **2016**, *66* (321), e074-e074.

(24) León-Martínez, F. M.; Cano-Barrita, P. F. d. J.; Lagunez-Rivera, L.; Medina-Torres, L. Study of nopal mucilage and marine brown algae extract as viscosity-enhancing admixtures for cement based materials. *Construction and Building Materials* **2014**, *53*, 190-202. DOI: https://doi.org/10.1016/j.conbuildmat.2013.11.068.
(25) Lin, M.-Y.; Grandgeorge, P.; Jimenez, A. M.; Nguyen, B. H.; Roumeli, E. Long-Term Hindrance Effects of Algal Biomatter on the Hydration Reactions of Ordinary Portland Cement. *ACS Sustainable Chemistry & Engineering* **2023**.
(26) Chen, X.; Matar, M. G.; Beatty, D. N.; Srubar III, W. V. Retardation of portland cement hydration with photosynthetic algal biomass. *ACS Sustainable Chemistry & Engineering* **2021**, *9* (41), 13726-13734.
(27) Chen, X.; Beatty, D. N.; Matar, M. G.; Cai, H.; Srubar III, W. V. Algal Biochar-Metal Nanocomposite Particles Tailor the Hydration Kinetics and Compressive Strength of Portland Cement Paste. *ACS Sustainable Chemistry & Engineering* **2024**, *12* (9), 3585-3594.
(28) Zhang, C.; Zhang, L.; Gao, J.; Zhang, S.; Liu, Q.; Duan, P.; Hu, X. Evolution of the functional groups/structures of biochar and heteroatoms during the pyrolysis of seaweed. *Algal research* **2020**, *48*, 101900.
(29) Bird, M. I.; Wurster, C. M.; de Paula Silva, P. H.; Bass, A. M.; De Nys, R. Algal biochar–production and properties. *Bioresource technology* **2011**, *102* (2), 1886-1891.
(30) Gupta, S.; Palansooriya, K. N.; Dissanayake, P. D.; Ok, Y. S.; Kua, H. W. Carbonaceous inserts from lignocellulosic and non-lignocellulosic sources in cement mortar: preparation conditions and its effect on hydration kinetics and physical properties. *Construction and Building Materials* **2020**, *264*, 120214.
(31) You, S.; Ok, Y. S.; Chen, S. S.; Tsang, D. C.; Kwon, E. E.; Lee, J.; Wang, C.-H. A critical review on sustainable biochar system through gasification: Energy and environmental applications. *Bioresource technology* **2017**, *246*, 242-253.
(32) Kim, K. H.; Kim, J.-Y.; Cho, T.-S.; Choi, J. W. Influence of pyrolysis temperature on physicochemical properties of biochar obtained from the fast pyrolysis of pitch pine (Pinus rigida). *Bioresource technology* **2012**, *118*, 158-162.
(33) Igalavithana, A. D.; Mandal, S.; Niazi, N. K.; Vithanage, M.; Parikh, S. J.; Mukome, F. N.; Rizwan, M.; Oleszczuk, P.; Al-Wabel, M.; Bolan, N. Advances and future directions of biochar characterization methods and applications. *Critical reviews in environmental science and technology* **2017**, *47* (23), 2275-2330.
(34) Walton, K. S.; Abney, M. B.; LeVan, M. D. CO2 adsorption in Y and X zeolites modified by alkali metal cation exchange. *Microporous and mesoporous materials* **2006**, *91* (1-3), 78-84.
(35) Yuan, J.-H.; Xu, R.-K.; Zhang, H. The forms of alkalis in the biochar produced from crop residues at different temperatures. *Bioresource technology* **2011**, *102* (3), 3488-3497.
(36) Johari, M. M.; Brooks, J.; Kabir, S.; Rivard, P. Influence of supplementary cementitious materials on engineering properties of high strength concrete. *Construction and Building Materials* **2011**, *25* (5), 2639-2648.
(37) Roy, D.; Arjunan, P.; Silsbee, M. Effect of silica fume, metakaolin, and low-calcium fly ash on chemical resistance of concrete. *Cement and Concrete Research* **2001**, *31* (12), 1809-1813.
(38) Zhang, M.-H.; Gjørv, O. E. Effect of silica fume on cement hydration in low porosity cement pastes. *Cement and concrete research* **1991**, *21* (5), 800-808.
(39) Everett, D. H. Manual of symbols and terminology for physicochemical quantities and units, appendix II: Definitions, terminology and symbols in colloid and surface chemistry. *Pure and Applied Chemistry* **1972**, *31* (4), 577-638.
(40) Li, Y.; Liu, L.; Yu, H.; Zhao, Y.; Dai, J.; Zhong, Y.; Pan, Z.; Yu, H. Synergy of developed micropores and electronic structure defects in carbon-doped boron nitride for CO2 capture. *Science of The Total Environment* **2022**, *811*, 151384.

(41) Guo, L.; Yang, J.; Hu, G.; Hu, X.; Wang, L.; Dong, Y.; DaCosta, H.; Fan, M. Role of hydrogen peroxide preoxidizing on CO2 adsorption of nitrogen-doped carbons produced from coconut shell. *ACS Sustainable Chemistry & Engineering* **2016**, *4* (5), 2806-2813.
(42) Huang, Y.-F.; Chiueh, P.-T.; Shih, C.-H.; Lo, S.-L.; Sun, L.; Zhong, Y.; Qiu, C. Microwave pyrolysis of rice straw to produce biochar as an adsorbent for CO2 capture. *Energy* **2015**, *84*, 75-82.
(43) Mochizuki, Y.; Bud, J.; Byambajav, E.; Tsubouchi, N. Pore properties and CO2 adsorption performance of activated carbon prepared from various carbonaceous materials. *Carbon Resources Conversion* **2024**, 100237.
(44) Guo, S.; Li, Y.; Wang, Y.; Wang, L.; Sun, Y.; Liu, L. Recent advances in biochar-based adsorbents for CO2 capture. *Carbon Capture Science & Technology* **2022**, 100059.
(45) Mantellato, S.; Palacios, M.; Flatt, R. J. Reliable specific surface area measurements on anhydrous cements. *Cement and Concrete Research* **2015**, *67*, 286-291.
(46) Yan, Y.; Geng, G. Evolution of CSH morphology at early age: New insights from direct TEM observation. *Journal of Building Engineering* **2023**, *73*, 106764.
(47) Richardson, I. G. The nature of CSH in hardened cements. *cement and concrete research* **1999**, *29* (8), 1131-1147.
(48) Richardson, I. G. Model structures for c-(a)-sh (i). *Acta Crystallographica Section B: Structural Science, Crystal Engineering and Materials* **2014**, *70* (6), 903-923.
(49) Kumar, A.; Walder, B. J.; Kunhi Mohamed, A.; Hofstetter, A.; Srinivasan, B.; Rossini, A. J.; Scrivener, K.; Emsley, L.; Bowen, P. The atomic-level structure of cementitious calcium silicate hydrate. *The Journal of Physical Chemistry C* **2017**, *121* (32), 17188-17196.
(50) Singh, R.; Balagurumurthy, B.; Bhaskar, T. Hydrothermal liquefaction of macro algae: effect of feedstock composition. *Fuel* **2015**, *146*, 69-74.

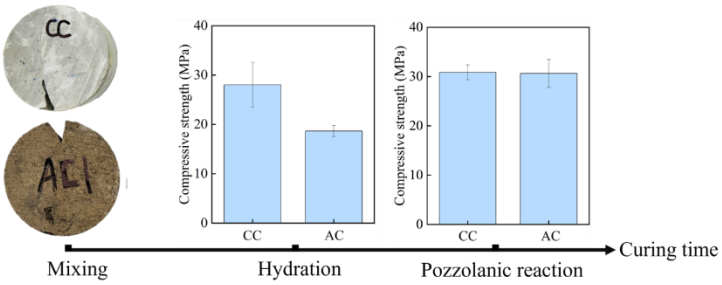

809

810 For Table of Contents Only

811

812 **Synopsis**: Algae-based biochar can reduce concrete's carbon footprint and cost while offering a
813 sustainable use for biofuel production waste.

814